RSC Advances

ROYAL SOCIETY OF CHEMISTRY

www.rsc.org/advances

RSC Advance

RSCPublishing

Paper

Mg doping in nanosheet-based spherical structured ZnO photoanode for quasi-solid dye-sensitized solar cells

Cite this: DOI: 10.1039/x0xx00000x

Received 00th January 2014,
Accepted 00th January 2014

DOI: 10.1039/x0xx00000x

www.rsc.org/

Xudong Guo,[a] Haopeng Dong,[a] Guangda Niu[a] Yong Qiu,[a] and Liduo Wang.*[a]

In this paper, Mg doping is utilized in the synthesis of nanosheet-based spherical structured ZnO photoanode resulting in the increased overall efficiency from 1.72% to 4.19% of quasi-solid dye-sensitized solar cells. Existence of Mg in ZnO crystal is detected by XRD and XPS measurement. The diameter of ZnO nanosheet-based spherical structure is obviously decreased after Mg doping, which facilitates the fabrication of ZnO films and increases the specific area leading to larger dye loading and higher photocurrent. The energy bandgap of ZnO photoanode with and without Mg doping is investigated by UV-vis spectra and theoretical calculation based on GAUSSIAN 09 program and an increase of bandgap is observed after Mg doping, which leads to an increase of conduction band position and enhances the photo-voltage of DSSCs based on Mg doped ZnO photoanode. An electrochemical impedance spectroscopy (EIS) test also indicates that DSSCs based on Mg doped ZnO shows a strengthened effect of facilitating electron transport and retarding the charge recombination

1.Introduction

Dye-sensitized solar cells (DSSCs) based on wide bandgap metal oxide nanocrystalline semiconductors as photoanodes have provided a promising option to the photovoltaic devices because of their simple fabrication processes and low cost. Until now, DSSCs fabricated by TiO_2 electrodes and liquid electrolytes have achieved an overall photoelectric conversion efficiency of 12.3%.[1] Compared with commonly used TiO_2 photoanodes, ZnO photoanodes have been widely investigated owing to its similar bandgap, easier synthesis process, higher electron mobility and controllable structure.[2-5] Thus ZnO nanotubes, nanorods, nanowires, nanosheets and other hierarchical structure based photoanodes have been fabricated and are expected to obtain high photoelectric conversion efficiencies when used in DSSCs.[6-10]

Hierarchical structured ZnO such as nanocrystalline aggregates,[11] dendritic nanowires[12] and flower-like spheres[13] have been reported in recent years. Nanosheet-based spherical structured ZnO can be synthesized by the following methods: hydrotherm,[14] chemical bath deposition,[15] electrodeposition,[16] direct precipitation,[17] and so on. Among these methods, one-step direct precipitation is the simplest approach and DSSCs based on Nanosheet-based spherical structure ZnO synthesized by this method have been proved to reach high efficiency.[18] However the size of nanosheet-based ZnO spheres synthesized by direct precipitation is about 4~5 um,[18] which is too large that the ZnO spheres are easy to assemble together and can't form homogenous and smooth films. Thus, ZnO nanopaticles (10-20wt%) about 20nm in diameter are needed to blend together with Nanosheet-based spherical structured ZnO to increase the mechanic strength of the photoanodes, which made the process complicated.

In addition to morphology controlling of ZnO, the metal doping is also an alternative method to improve the DSSCs' performance.[19-23] Doped ZnO thin films exhibit relatively low resistivity, high transmittance and chemical stability when compared with pure ZnO thin films. Former work has reported a banyan root like Mg-doped ZnO photoanode based DSSCs' conversion efficiency of 4.11% under 1 sun illumination.[24] However, in that work, Mg doping is achieved by the introduction of the appropriate amount of magnesium acetate dihydrate and zinc acetate adding into 2-methoxyethanol and monoethanolamine, which may lead to the formation of ZnO and MgO separately, thus weaken the effect of Mg doping.

Here we report a new method to synthesis Mg doped nanosheet-based spherical structured ZnO and fabricated DSSCs. In this work, Zn^{2+} is firstly reacted with OH^- forming $[Zn(OH)_4]^{2-}$, then mixed with Mg^{2+} to form Mg doped ZnO. By Mg doping, the diameter is obviously reduced, which facilitate the formation of ZnO films and simplified the photoanode fabrication process. The photo-electric properties of ZnO DSSCs such as photocurrent and photo-voltage are obviously improved after Mg doping and the reasons for these improvements are investigated in this paper. Quasi-solid electrolytes were used here to avoid the problems such as

electrolyte leakage, volatilization and corrosion that limiting the long-term performance of the DSSCs assembled using liquid electrolytes.[18]

2.Experiment

2.1 Synthesis of Mg doped ZnO Particles and Fabrication of Photoanode

ZnO and Mg doped ZnO containing hierarchic structures are synthesized by a direct precipitation method, and reactants are used without further purification. Firstly, 4.39g zinc nitrate hexahydrate (1M), 4.8g sodium hydroxide (4M) and 2.58g sodium citrate(1M) are dissolved in 20mL, 30mL, and 10mL distilled water separately. The above three solutions are bathed in ice water bathe for 15 min to ensure the temperature of them is below 5 centigrade and then are mixed together. White deposits appear at first, after stirring for 1 min the deposits disappear and the mixed $[Zn(OH)]^{2-}$ solution is transparent again. Then the $[Zn(OH)]^{2-}$ solution is added to the 500mL 0% or 2% magnesium acetate aqueous solution with heavily stirring at 30 centigrade. After stirring for 1h, the resulting white product is filtered and ished with distilled water and ethanol for 2 times separately. In our experiment, the doctor-blade technique is used to prepare the porous ZnO layer on an FTO glass substrate with the thickness being controlled by a 15um.

2.2 Assembly of the DSSCs

The ZnO photoanode is sintered at 200 ℃ then sensitized in 0.3mM N719 absolute ethanol solution for 100min, followed by cleaning with absolute ethanol. A chemically platinized conductive glass is used as the counter electrode. The composition of the polymer gel electrolyte is LiI (0.1M), I2(0.1M), 1,2-dimethyl-3-propyl imidazolium iodide (0.6M), and N-methyl-benzimida-zole (0.45M); the solvent is 3-methoxypropionitrile, and the PEO (molecular weight , Mw=2 ×106 g mol-1) weight ratio (versus liquid electrolyte) is 10%. When assembling the DSSCs, the polymer gel electrolyte is sandwiched by a sensitized ZnO electrode and a counter electrode with two clips; the space between the two electrodes is controlled by an adhesive tape with a thickness of 30mm, and the DSSC is not sealed. Finally, the DSSC is baked at 80℃ to ensure the polymer gel electrolyte can penetrate into the nanoporous electrode.

2.3 Characterization

Morphologies of the ZnO particles and the photo-anodes are characterized by SEM (JSM 7401). The photovoltaic performance of the DSSCs is measured by KEITHLEY 4200 under solar simulator (Xenon lamp, Oriel, AM 1.5, 30 or 100mW cm), and the incident light intensity is calibrated with a standard crystalline silicon solar cell. BET analysis is performed by a Mercury Porosimeter (Quantachrome, Autoscan-33).The total active area of the DSSCs is 0.16 cm^{-2}; three DSSCs are assembled for each sample and the intermediate value of the conversion efficiencies is used in this paper. The bias voltage for EIS measurement (CHI660 electrochemical work station, USA) is the open-circuit voltage, and the frequency ranged from 0.05 to 10^5 Hz. The IPCE is measured by using a lab-made IPCE setup in Prof. QingboMeng's lab in Institute of Physics, Chinese Academy of Sciences.

3. Results and Discussion

3.1 Influence of the Mg doping on the ZnO photoanode struture and dye loading

Fig.1 is the scanning electron microscopy (SEM) images showing the morphologies of the ZnO films and 2% Mg doped ZnO films. These films consist of microspheres assembled by ZnO nanosheets interlaced with each other. Mg dope ZnO's diameter is about 1 um, which is obviously smaller than ZnO's 4 um without Mg doping. That is because the existence of magnesium acetate accelerates the formation of ZnO. Equation (1) and (2) show the chemical reactions in $[Zn(OH)_4]^{2-}$ solutions with and without magnesium acetate.

$$(1-x)[Zn(OH)_4]^{2-} + xMg(Ac)_2 = Zn_{1-x}Mg_xO + 2xAc^- + H_2O + (2-4x)OH^- \quad (1)$$

$$[Zn(OH)_4]^{2-} = ZnO + H_2O + 2OH^- \quad (2)$$

The reaction rate in equation (2) is very low but in equation (1) the acid magnesium acetate can act as the reaction center to congregate $[Zn(OH)_4]^{2-}$, which quickens the reaction. Fig.2 shows the formation process of ZnO with Mg doping and withot Mg doping. In the Mg^{2+} absent system, the repulsion between $[Zn(OH)_4]^{2}$- makes the process of ZnO crystal nucleus formation slow and only a few ZnO crystal nucleus generate. When adding Mg^{2+} in to this system, Mg^{2+} would attract the OH- of $[Zn(OH)_4]^{2-}$ because the solubility product (Ksp) of $Mg(OH)_2$ is only 1.8×10^{-11}. As a result, the equilibrium in the $[Zn(OH)_4]^{2-}$ is broken rapidly and a large amount of $Zn_{1-x}Mg_xO$ crystal nucleus appears. As the quantity of $[Zn(OH)_4]^{2-}$ is equal in both these two systems, the ZnO nanoparticle is much larger in the Mg^{2+} absent system as showed in Fig. 2. As for the

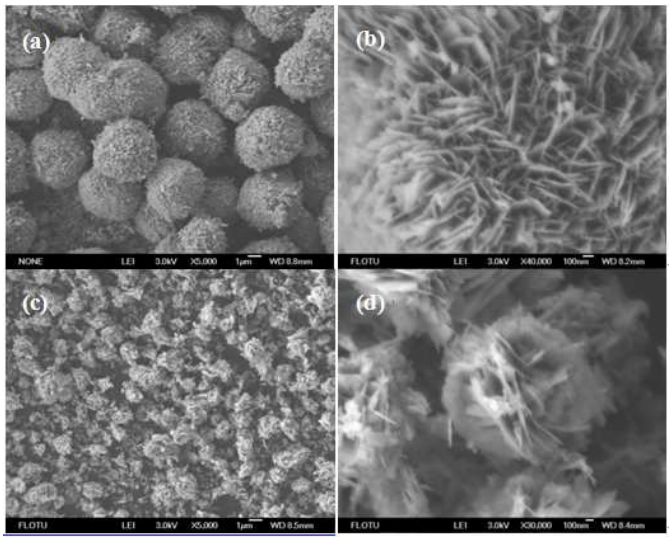

Fig. 1 SEM images of (a) (b) ZnO photoanode and (c) (d)2 mol %,Mg-doped ZnO photoanodes.

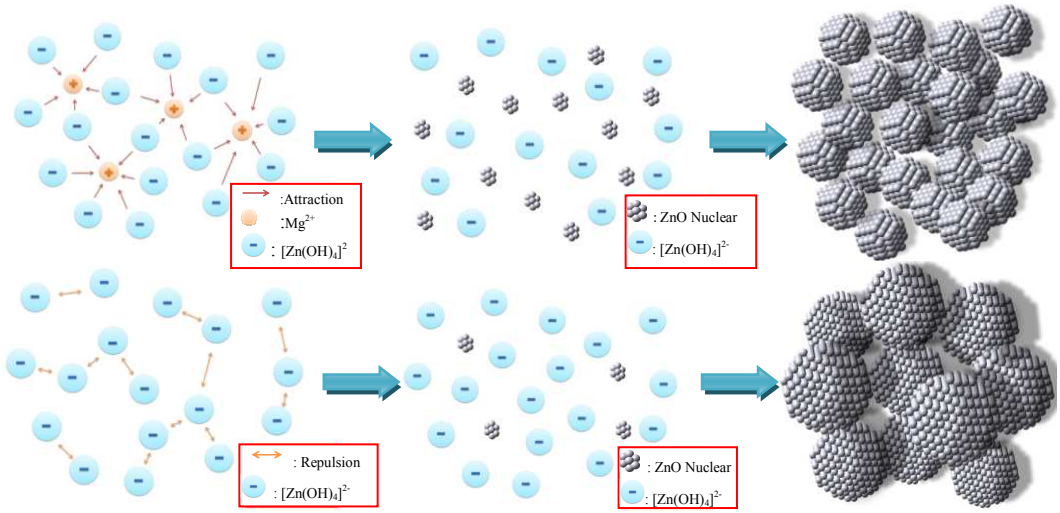

Fig. 2 Schematic diagram of ZnO formation process with Mg doping (top) and without Mg doping (bottom)

nanosheet structure, the driving forces to assemble nanocrystals are anisotropic hydrophobic attraction and electro-static interactions derived from dipole moments or surface charges, which makes ZnO form nanosheet structure.[18]

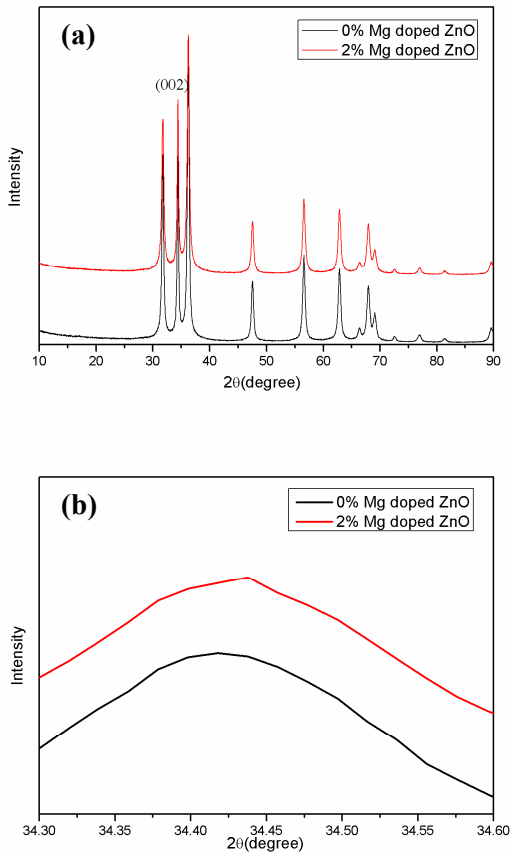

Fig 3.(a) XRD pattern of ZnO with and without Mg doping on FTO substrate. (b) Shift of (002) peak position of ZnO with and without Mg doping

Fig. 3a shows the X-ray diffraction patterns of Mg doped ZnO and pure ZnO films on FTO substrate. As seen in this figure, the films are polycrystalline with hexagonal wurtzite structure without any new phase due to the addition of Mg. The shift of the corresponding (002) peak toward higher angle (Fig. 3b) is mainly due to the incorporation of Mg ions in the interstitial sites of wurtzite structure. The ion radius of Mg^{2+} is less than that of Zn^{2+}, which would decrease the spacing of ZnO crystal. According to the Braggs Formula:

$$2d\sin\theta=n\lambda \quad (3)$$

where n is an integer, λ is the wavelength of incident wave, d is the spacing between the planes in the atomic lattice, and θ is the angle between the incident ray and the scattering planes. The decrease of d (crystal spacing distance) would lead to the increase of θ (crystal dihedral), cooperating well with Fig. 3b**.**

XPS was measured to investigate the composition and chemical bond configuration of pure and Mg doped ZnO thin films. Fig. 4 is the typical XPS survey spectra of pure and

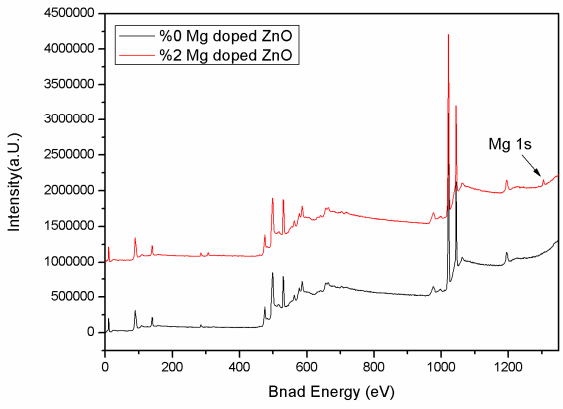

Fig 4. XPS survey of ZnO with and without Mg doping on FTO substrate

Mg doped ZnO thin films, showing the Mg 1s binding energy peak at 1304.27 eV in the Mg doped ZnO thin film but no such peak in pure ZnO films, which confirmed that Mg was doped into the ZnO. By integrating the XPS peak area, the atomic percent of Mg and Zn is 3.73% and 43. 78%, respectively. That means after reaction, the mole percent of Mg increased from 2% to about 8%. In equation (4), the $Zn(OH)_4^{2-}$ can't react completely because increase of OH^- would retard this reaction moving forward.

N3 adsorption/desorption is used to detect the specific area of the photoanodes based on two samples and the results are shown in Table 1. We can see that after Mg doping, specific areas of the samples increased from 16.83 $m^2 g^{-1}$ to 37.12 $m^2 g^{-1}$, in accordance with their particle sizes, proving that Mg doping can increase nanosheet-based spherical ZnO' specific areas on a large scale. The amount of dye adsorbed on ZnO and Mg doped

ZnO electrodes is estimated by desorbing the dye from sensitized ZnO phtoanode using sodium hydrate. Compared to pure ZnO film (Fig.2), Mg doped ZnO electrodes shows an increased dye adsorption. Detailed data is listed in Table 1. The dye-loading of pure ZnO is 104 nmol cm^{-2} and increased to 155 nmol cm^{-2} after Mg doping. This larger dye adsorption in Mg doped ZnO will lead to a higher photocurrent when fabricated DSSCs. However, the value of specific area is not proportionate to that of Dye-loading. That is because the resistance of ZnO electrode surface to acidic dye increased after Mg doping.[24]

3.2 Influence of the Mg doping on the ZnO photoanode energy band gap

Table.1 BET and Dye loading Parameters of DSSCs based on ZnO and Mg doped ZnO

Samples	Specific area/m^2·g-1	Dye-loading/nmol·cm^{-2}
ZnO	16.83	104
Mg doped ZnO	37.12	155

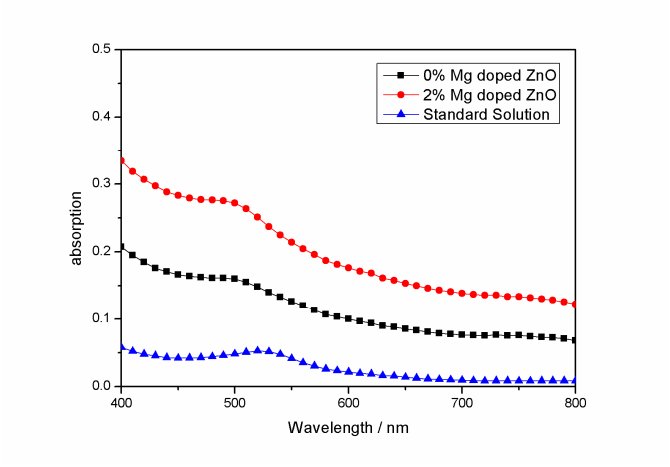

Fig. 5 UV-Vis absorbance spectra of solutions containing dyes desorbed from the sensitized photoanodes composed of ZnO with and without Mg doping

In ZnO based DSSCs, the electron is first excited to the LUMO of the dye molecular after illumination and then inject into the conduction band of ZnO photoanode. Thus the position of the conduction band is important for the photoelectric conversion process. The conduction band of ZnO is composed by the empty 4s orbit of Zn atom. After Mg doping, the conduction band of ZnO is tuned by the orbit of Mg atom. However, the valance band of ZnO is composed by the orbit of O atom and will not change after Mg doping. Thus, the variation of the conduction band can be conjectured by the variation of band gap. Here we use UV-vis DRS(diffuse reflectance spectroscopy) spectra and theoretical calculation to investigate the variation of band gap.

According to former research, the optical band gap(Eg) of metal oxide semiconductor Eg for the absorption edge and the absorption coefficient(A) near the photo absorption edge has a relationship complied with the following formula:[24]

$$(Ahv)^2 = c(hv-Eg) \quad (4)$$

From equation (4) we can find that the Eg for the absorption edge can be obtained by fitting linear portion (3.25eV to 3.31eV for undoped ZnO and 3.29eV to 3.32eV for Mg doped ZnO) with least square method. The correlation coefficients are 0.985 and 0.991respectively. In Fig.6, after Mg doping, the bandgap of ZnO increases from 3.23eV to 3.27eV indicating a 0.04eV's rise of the ZnO photoanode's conduction band position. The photo-voltage of a DSSCs corresponds to the difference of the quasi-Fermi level of electrons in the photoanode under illumination and the Nernst potential of the electrolyte. As the Nernst potential of the electrolyte remains the same, the photo-voltage increases because of the rise of the conduction band after Mg doping.

Furthermore, we execute theoretical calculation to investigate the band gap change of Mg doped ZnO. Calculations are performed with the help of DFT at the B3LYP level and the GAUSSIAN 09 program.[25] The B3LYP functional[24] has been shown to provide realistic bulk band gap energies of metal oxides, and is thought to work well also for nanosized clusters. Both Zn atoms and O atoms are presented by the 6-31+g* basis set, which includes one polarized[26] and

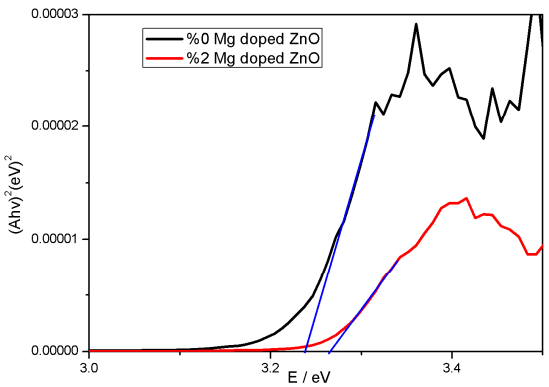

Fig. 6 $(Ahv)^2$ vs hv curves of ZnO with and without Mg doping from UV-vis DRS spectra

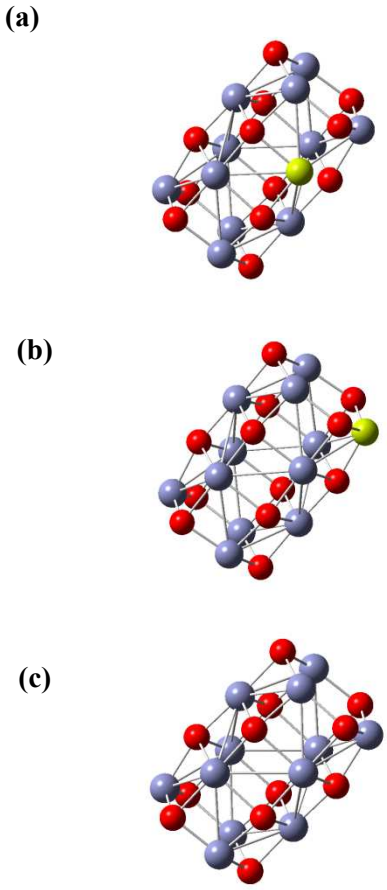

Fig. 7 optimized configuration of (a) Mg doped ZnO cluster 1 (b) Mg doped ZnO cluster 2 and (c) pure ZnO cluster1 calculated by b3lyp DFT method, red spheres represent O, blue spheres represent Zn and yellow spheres represent Mg

one diffused function[27]. Because the atomic percent of Mg and Zn is 3.73% and 43. 78%, the real atomic ratio between Mg and Zn is about 1：11. According to this ratio, the following three initial configurations were choosen, which is built from cutting wurzite-ZnO crystal, comes from Zhao et al.'s work to design and character ZnO clusters.[28] Fig.6 shows the optimized configuration. The calculated Mg doped ZnO's HOMO-LUMO gap(band gap) increases from 3.79eV to 3.84eV (Fig 7a's configuration) and 3,85 (Fig 7b's configuration), indicating a 0.05—0.06eV's rise of the ZnO photoanode's conduction band after Mg doping. This increment corresponds to the value investigated by UV-vis DRS spectra very well and will express on the photo-voltage's increase of DSSCs in the next section.

3.3 Influence of the Mg doping on the Devices' Photovoltaic Performance

To investigate the performance variation caused by Mg doping, ZnO and Mg doped ZnO are assembled into DSSCs for further study. Under AM 1.5, 100 mW cm^{-2} light illumination, the performances of these two series of photoanodes are measured and illustrated in Fig. 8 with detailed parameters summarized in Table 2. The DSSCs devices based on Mg doped ZnO performed much better than that based on pure ZnO. The short current density (*Jsc*) increases from 6.08 to 11.18 $mA{\cdot}cm^{-2}$ after Mg doping due to the larger specific area and more dye-loading, which is investigated in the first section. The open circuit voltage (V*oc*) increase from 0.56V to 0.60V mainly because the conduction band of Mg doped ZnO is higher than pure ZnO, which is investigated in the second section. The fill factor (FF) increased from 50.1% to 62.5% owing to the larger interface resistance between photoanode and electrolyte of Mg doped ZnO. As a result, the overall efficiency exhibited a remarkable 143% enhancement increasing from 1.72% to 4.19% after Mg doping.

Table.2 Parameters of DSSCs based on ZnO film with and without Mg doping

Samples	Jsc/($mA{\cdot}cm^{-2}$)	Voc/V	FF%	η%
ZnO	6.08	0.56	50.1	1.72
Mg doped ZnO	11.18	0.60	62.5	4.19

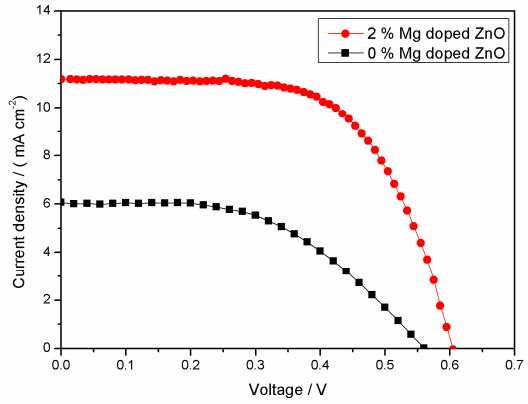

Fig. 8 Current–voltage (I–V) characteristics of DSSCs based on a ZnO film with and without Mg doping

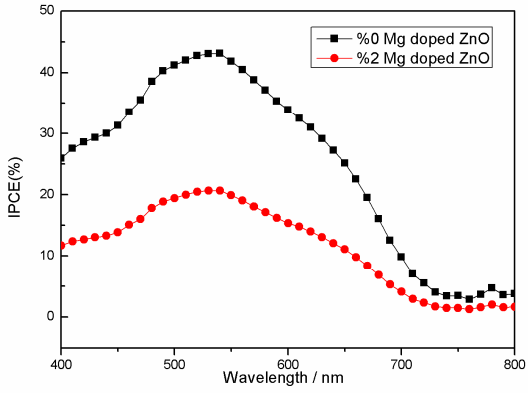

Fig. 9 IPCE spectrum of ZnO DSSCs with and without Mg doping

To investigate the reasons for a higher photocurrent result for DSSCs based on Mg doped ZnO, we measured the monochromatic incident photon-to-current conversion efficiency (IPCE) to study the photoactive wavelength regime for the pure and doped ZnO cells. The IPCE value is the percentage of photons hitting the device's photoreactive surface that produce charge carriers at FTO. At approximately 520nm, there is an obvious enhancement of Mg doped ZnO's IPCE value compared to the pure ZnO's value, which is attributed to the more dye adsorption and less recombination of electrons with the electrolyte mainly due to the larger resistance at the interface of photoanode and the electrolyte.

In order to estimate the resistance of electron transport and charge recombination processes in Mg doped and pure ZnO DSSCs, we have measured the electrochemical impedance spectra (EIS) under fixed illumination of 100mWcm^{-2}. The Nyquist plots of the DSSCs under dark and sun condition are shown in Fig. 10, where the equivalent circuit of the DSSCs is inserted. On the equivalent circuit, the series resistance (R_S) includes the FTO electrode and external circuit while other three impedance units represent resistances (R_1, R_2, R_3) and constant phase elements (CPE_1, CPE_2). The diameters of the

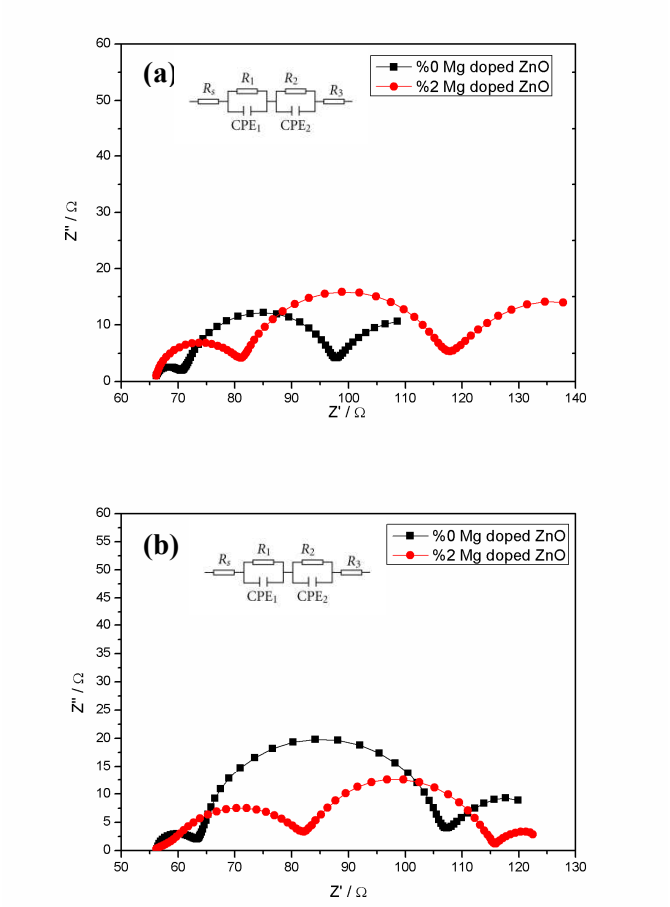

Fig. 10 EIS of ZnO DSSCs with and without Mg doping at (a) dark and (b) sun condition

semicircles (Fig. 10) at high, intermediate, and low frequency ranges represent R_1, R_2,and R_3, corresponding to the resistances for the charge transfer at the counter electrode, the electron ransport/charge recombination at the ZnO/electrolyte interface, and the diffusion of I^{3-} ions in the electrolyte, respectively.[29]

Fig. 10a shows the Nyquist plots of devices based on ZnO and Mg doped ZnO at open-circuit voltage in dark condition, where the diameter of middle frequency semicircle represents the resistance of at the sensitized Mg doped ZnO/electrolyte interface. Compared with pure ZnO, the interface resistance (R_2) of Mg doped ZnO based DSSCs is larger, which means the charge recombination at the ZnO/dye/electrolyte interface is obviously retarded and as a result to improve the electron collection. The decrease of recombination is mainly caused by an increase in electron lifetime supports reduction in the recombination of injected electrons with the I^{3-} in the electrolyte.[24] Under illumination condition, the DSSCs could be taken as diodes and resistanceat the ZnO/dye/electrolyte interface is also presented by the middle frequency semicircle in the Nyquist plots.[30] As shown in Fig. 10(b), The smaller the diameter of middle frequency semicircle shows a smaller interface resistance and a faster electron injection at the sensitized Mg doped ZnO/electrolyte interface, which is supposed to be the main reason an increase in fill factor from 50.1% to 62.5%.. Thus the enhanced injection electron can raise the photo-current and IPCE, which accorded with the results shown in Fig. 8, Fig. 9 and Tabel. 2.

4. Conclusion

Nanosheet-based sphirecal structured Mg doped ZnO photoanode is synthetized and shows a better performance than bare ZnO. The diameter of ZnO nanosheet-based hierachial structure is decreased from 4um to 1um after Mg doping, which facilitates the fabrication of ZnO films and increase the specific area from 16.83 $m^2 \cdot g^{-1}$ to 37.12 $m^2 \cdot g^{-1}$, leading to more dye loading and higher photocurrent. The energy bandgap of ZnO photoanode with and without Mg doped are investigated by UV-vis spectra and theoretical calculation based on GAUSSIAN 09 program and an increase of bandgap is observed after Mg doping, which leads to the increase of photovoltage of DSSCs based on Mg doped ZnO photoanode. As a result, the short current density (J*sc*), open circuit voltage (V*oc*), overall efficiency increase from 6.08 to 11.18 mA·cm^{-2} , 0.56 to 0.60V, 1.72% to 4.19%, respectively. An electrochemical impedance spectroscopy (EIS) test also indicated that DSSCs based on Mg doped ZnO shows a strengthened effect of facilitating electron transport and retarding the charge recombination. With the optimization of the Mg doping content and device fabrication, further enhancement in power conversion efficiency is expected.

Acknowledgements

This work is supported by the National Natural Science Foundation of China under Grant no. 51273104 and the National Key Basic Research and Development Program of China under Grant no. 2009CB930602.

Notes and references

[a] *Key Lab of Organic Optoelectronics & Molecular Engineering of Ministry of Education, Department of Chemistry, Tsinghua University, Beijing 100084, China*
E-mail: chldwang@mail.tsinghua.edu.cn

1. A. Yella, H. W. Lee, H. N. Tsao, C. Y. Yi and A. K. Chandiran, *Science*, 2011, **334**, 1203-1203.
2. M. Law, L. E. Greene, A. Radenovic, T. Kuykendall, J. Liphardt and P. Yang, *J. Phys. Chem. B*, 2006, **110**, 22652-22663.
3. A. B. F. Martinson, J. W. Elam, J. T. Hupp and M. J. Pellin, *Nano Lett.*, 2007, **7**, 2183-2187.
4. Q. Zhang, T. R. Chou, B. Russo, S. A. Jenekhe and G. Cao, *Angew. Chem. Int. Ed.*, 2008, **47**, 2402-2406.
5. Q. Zhang, C. S. Dandeneau, X. Zhou and G. Cao, *Adv. Mater.*, 2009, **21**, 4087-4108.
6. J. B. Baxter, A. M. Walker, K. van Ommering and E. S. Aydil, *Nanotech.*, 2006, **17**, S304-S312.
7. T. P. Chou, Q. Zhang, G. E. Fryxell and G. Cao, *Adv. Mater.*, 2007, **19**, 2588-2592.
8. E. Galoppini, J. Rochford, H. Chen, G. Saraf, Y. Lu, A. Hagfeldt and G. Boschloo, *J. Phys. Chem. B*, 2006, **110**, 16159-16161.
9. K. Keis, C. Bauer, G. Boschloo, A. Hagfeldt, K. Westermark, H. Rensmo and H. Siegbahn, *J. Photochem. Photobiol., A*, 2002, **148**, 57-64.
10. M. Quintana, T. Edvinsson, A. Hagfeldt and G. Boschloo, *J. Phys. Chem. B*, 2007, **111**, 1035-1041.
11. J. Shi, Y. Liu, Q. Peng and Y. Li, *Nano Res.*, 2013, **6**, 441-448.
12. F. Hong Jin, R. Scholz, F. M. Kolb and M. Zacharias, *Appl. Phys. Lett.*, 2004, **85**, 4142-4144.
13. M. Thambidurai, N. Muthukumarasamy, D. Velauthapillai and C. Lee, *J. Mater. Sci. - Mater. Electron.*, 2013, **24**, 2367-2371.
14. Z. Li, Y. Zhou, G. Xue, T. Yu, J. Liu and Z. Zou, *J. Mater. Chem.*, 2012, **22**, 14341-14345.
15. E. Hosono, S. Fujihara and T. Kimura, *Electrochim. Acta*, 2004, **49**, 2287-2293.
16. X. Lifen, C. Qingwei and X. Dongsheng, *J. Phys. Chem. C*, 2007, **111**, 11560-11565.
17. C. Cheng, Y. Shi, C. Zhu, W. Li, L. Wang, K. K. Fung and N. Wang, *Phys. Chem. Chem. Phys.*, 2011, **13**, 10631-10634.
18. Y. Shi, C. Zhu, L. Wang, C. Zhao, W. Li, K. K. Fung, T. Ma, A. Hagfeldt and N. Wang, *Chem. Mater.*, 2013, **25**, 1000-1012.
19. J. Chang, Z. Lin, C. Zhu, C. Chi, J. Zhang and J. Wu, *ACS Appl. Mater. Interfaces*, 2013, **5**, 6687-6693.
20. H. Chia-Cheng, W. Fang-Hsing and Y. Chen-Fu, *Appl. Phys. A*, 2013, **112**, 877-883.
21. A. Gadisa, T. Hairfield, L. Alibabaei, C. L. Donley, E. T. Samulski and R. Lopez, *ACS Appl. Mater. Interface*, 2013, **5**, 8440-8445.
22. J. Xie, C. Guo and C. M. Li, *Phys. Chem. Chem. Phy.*, 2013, **15**, 15905-15911.
23. J.-X. Zhao, X.-H. Lu, Y.-Z. Zheng, S.-Q. Bi, X. Tao, J.-F. Chen and W. Zhou, *Electrochem. Commun.*, 2013, **32**, 14-17.
24. C. J. Raj, K. Prabakar, S. N. Karthick, K. V. Hemalatha, M.-K. Son and H.-J. Kim, *J. Phys. Chem. C*, 2013, **117**, 2600-2607.
25. G. W. T. M. J. Frisch, H. B. Schlegel, G. E. Scuseria, M. A. Robb, J.R. Cheeseman, G. Scalmani, V. Barone, B. Mennucci, G. A. Petersson, H. Nakatsuji, M. Caricato, X. Li, H. P. Hratchian, A. F. Izmaylov, J. Bloino, G. Zheng, J. L. Sonnenberg, M. Hada, M. Ehara, K. Toyota, R. Fukuda, J. Hasegawa, M. Ishida, T. Nakajima, Y. Honda, O. Kitao, H. Nakai, T. Vreven, J. A. Montgomery, Jr., J. E. Peralta, F. Ogliaro, M. Bearpark, J. J. Heyd, E. Brothers, K. N. Kudin, V. N. Staroverov, R. Kobayashi, J. Nor-mand, K. Raghavachari, A. Rendell, J. C. Burant, S. S. Iyengar, J. Tomasi, M. Cossi, N. Rega, J. M. Millam, M. Klene, J. E. Knox, J. B. Cross, V. Bakken, C. Adamo, J. Jaramillo, R. Gomperts, R. E. Stratmann, O. Yazyev, A. J. Austin, R. Cammi, C. Pomelli, J. W. Ochterski, R. L. Martin, K. Morokuma, V. G. Zakrzewski, G. A. Voth, P. Salvador, J. J. Dannenberg, S. Dapprich, A. D. Daniels, ø. Farkas, J. B. Foresman, J. V. Ortiz, J. Cioslowski, and D. J. Fox, Gaussian 09; Gaussian Inc.:Gaussian Inc.:Wallingford, CT, 2009.
26. Harihara.Pc and J. A. Pople, *Thermochim. Acta*, 1973, **28**, 213-222.
27. T. Clark, J. Chandrasekhar, G. W. Spitznagel and P. V. Schleyer, *J. Comput. Chem.*, 1983, **4**, 294-301.
28. M. Zhao, Y. Xia, Z. Tan, X. Liu and L. Mei, *Phy.s Lett. A*, 2007, **372**, 39-43.
29. Z. Chao, S. Yantao, C. Chun, W. Lin, F. Kwok Kwong and W. Ning, *J. Nanomater.*, 2012, 212653 (212658 pp.)-212653 (212658 pp.).
30. R. Gao, G.-D. Niu, L.-D. Wang, B.-B. Ma and Y. Qiu, *Acta Phys-Chim. Sin.*, 2013, **29**, 73-81.

TOC

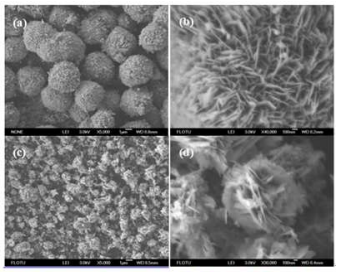

SEM images of (a) (b) ZnO photoanode and (c) (d)2 mol% Mg-doped ZnO photoanodes.

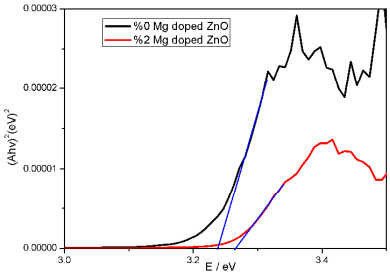

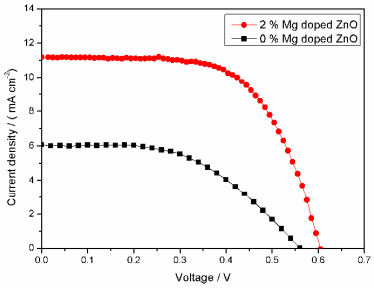

Mg doping is utilized in the synthesis of nanosheet-based spherical structured ZnO photoanode, resulting in the increased specific area, conduction band position and overall efficiency.